First principles simulations of the structural and electronic properties of silicon nanowires

T. Vo, A. J. Williamson,* and G. Galli
Lawrence Livermore National Laboratory, Livermore, California 94550, USA
(Received 22 December 2005; revised manuscript received 10 March 2006; published 19 July 2006)

We report the results of first principles studies of the structural and electronic properties of hydrogen-passivated silicon nanowires with [001], [011], and [111] growth directions and diameters ranging from 1 to 3 nm. We show that the growth direction, diameter, and surface structure all have a significant effect on the structural stability, electronic band gap, band structure, and band-edge effective masses of the nanowires. The band gap is found to decrease with increasing diameter and to be further reduced by surface reconstruction. While the electron and hole effective masses are found to depend on NW size for [001] and [111] NWs, they are almost independent of size for [011] NWs. Our results suggest the possibility of engineering the properties of nanowires by manipulating their diameter, growth direction, and surface structure. Finally, we use FEFF calculations to predict the extended x-ray absorption fine structure spectra produced by the relaxed atomic structure of the NWs and show that these spectra can serve as a tool for detecting surface reconstructions on NWs.

DOI: 10.1103/PhysRevB.74.045116 PACS number(s): 78.67.−n, 73.22.−f, 78.55.−m

Recent experiments have shown that small semiconducting nanowires (NWs) with various sizes, growth directions, and surface structures (reconstructed and nonreconstructed) can be successfully synthesized.[1–5] NWs exhibit quantum confinement effects, similar to quantum wells and quantum dots, in the directions perpendicular to the growth direction, and periodic band structures parallel to the growth direction. The perpendicular quantum confinement has been observed in photoluminescence studies that showed a substantial blueshift of emission with decreasing nanowire diameter.[6–8] Scanning tunneling spectroscopy data have also revealed a significant increase in the band gap as the size of the NW is decreased.[9] As a result of these tunable optoelectronic properties, NWs are being considered as potential candidates for a wide range of applications such as photovoltaic cells, photodetectors, field-effect transistors,[10,11] inverters,[12] light-emitting diodes, and nanoscale sensors.[13,14]

Among these many possible applications, there is particular interest in using NWs to fabricate thermoelectric materials.[15–17] The suitability of a material for thermoelectric applications is characterized by its figure of merit *ZT*,

$$ZT = \sigma T S^2/\kappa, \tag{1}$$

where S is the Seebeck coefficient, σ the electronic conductivity, and κ the thermal conductivity, which contains both electronic and lattice contributions, $\kappa=\kappa_e+\kappa_l$. The electronic conductivity is proportional to electron and hole mobilities, which are inversely proportional electron and hole masses. The electronic thermal conductivity depends on the electronic band structure, electron scattering, and electron-phonon interactions. The lattice conductivity depends mainly on the phonons (nuclear vibrations) and phonon scattering. Large *ZT* values require a high S, high σ, and low κ. Typically, an increase in σ also implies an increase in the electronic contribution to κ as given by the Wiedemann-Franz law, which is the main reason it is difficult to increase the value of *ZT*.

For five decades, many new materials have been investigated in the search for materials with a higher thermoelectric figure of merit *ZT*, but so far *ZT* has remained stuck in the range of ~0–1.[18] However, in recent years, experimental studies have shown that the value of *ZT* can be significantly improved by incorporating NWs into a material structure.[19] In these composite NW materials, quantum confinement provides a mechanism for engineering the electronic band structure, potentially reducing the electron and hole masses, thereby increasing their mobilities and increasing σ. Furthermore, the reduced size and dimension of the NWs increases the influence of the surfaces, leading to a significant modification of the vibrational properties (dispersion curve and/or relaxation time) by increasing the surface scattering of phonons, thus further decreasing thermal conductivity (κ_l) and increasing the thermoelectric figure of merit.[17,20–26] As all the parameters such as NW size, surface structures, and growth direction may affect the value of *ZT* by changing the electrical and thermal conductivity, to enable the design of optimal nanowire based thermoelectric materials, one must first develop a comprehensive understanding of how the structural, electronic, and transport properties depend on the size, growth direction, and structure of the NW.

Several previous studies have been performed to predict the effects of quantum confinement on the optoelectronic properties of semiconducting NWs.[27–32] However, these previous studies have mostly focused on explaining the photoluminescence of porous Si (Ref. 33) and predicting the electronic properties of unpassivated/passivated silicon nanowires grown in the [001] direction with an idealized, square cross section and small diameters.[27–31,34,35] One recent work by Zhao *et al.*[32] studied the effect of the size on the electronic properties of silicon NWs terminated with hydrogen in an idealized, symmetric dihydride structure. To our knowledge, the effect of surface reconstructions on the optoelectronic properties of hydrogen-terminated silicon NWs has yet to be studied.

In this paper, the effects of varying wire diameter, growth direction, and surface structure on the electronic, optical, and transport properties of hydrogen-passivated silicon NWs are systematically investigated using first principles calculations.

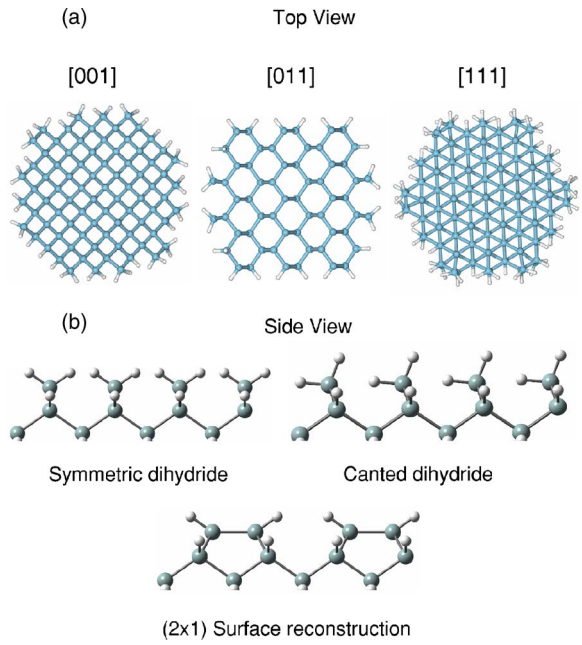

FIG. 1. (Color online) Fully relaxed 3 nm Si NWs: (a) in three different growth directions [001], [011], and [111], and (b) with three different surfaces.

The relative stabilities of NWs with different surface structures and growth directions are also discussed. We find that the NW stability, band gap, and effective mass all depend strongly not only on the size of the NWs but also on their growth directions and surface structures. We also find that surface reconstruction on the NWs can be detected by study of the changes in the extended x-ray absorption fine structure (EXAFS) spectra.

The rest of the paper is organized as follows. In Sec. I, we describe the details of how each hydrogen-terminated silicon NW geometry was constructed, and how the first principles calculations of the relaxed atomic geometry and electronic structure were performed. In Sec. II, we discuss the properties of the optimized NW geometries, their relative stabilities, and our predicted EXAFS absorption spectra for those geometries. In Sec. III, we describe the calculated electronic properties of the NWs, including their electronic density of states, band structures, band gaps, orbital densities, and electron and hole effective masses.

I. NANOWIRE STRUCTURES AND GEOMETRY OPTIMIZATION

We studied hydrogen-terminated silicon NWs grown along the [001], [011], and [111] directions, with diameters ranging from 1 to 3 nm. Three surface structures were considered: symmetric SiH_2 dihydrides, canted SiH_2 dihydrides, and a (2×1) surface reconstruction. Figure 1 shows end-on views of 2 nm NWs for each of the three growth directions [Fig. 1(a)] and each of the surface structures [Fig. 1(b)]. The sizes and symmetries of each of the NW structures are summarized in Table II.

For each NW, the atomic structure was initially constructed from diamond structure, bulk silicon. NW structures were chosen that most closely approximated a cylindrical geometry, i.e., the surface facets were chosen to approximate a circular cross section. The process of constructing the NW geometry was as follows: the structure of the silicon core of the NWs was constructed by selecting all the Si atoms that fall within a virtual cylinder placed in bulk silicon. All Si atoms falling outside this virtual cylinder were removed and the surface dangling bonds were terminated with hydrogen atoms placed at the Si-H distance in SiH_4. SiH_3 surface groups were removed as these were deemed too reactive. The diameter of the NW was varied by changing the diameter of the virtual cylinder. The direction of the cylinder was chosen to produce wires with [001], [011], and [111] growth directions. To select wire with high symmetry, we chose to align the central axis of the cylinder so that it either passed through an atom, the center of a Si-Si bond, or a high-symmetry center between atoms. For the smallest, 1.1 nm $[1\bar{1}1]$ NWs, it is not possible to generate structures with $\{0\bar{1}1\}$ facets containing SiH_2 dihydrides which can be reconstructed. Therefore, a larger 1.2 nm structure was used to make comparisons with larger systems.

The initial geometries were then relaxed to their closest, total energy minimum using the QBox Quantum Molecular Dynamics code,[36] in which density functional theory (DFT) is implemented within the LDA. In all cases, the structural relaxation was performed such that the forces on each atom are less than 0.001 eV/Å. A supercell approach was adopted where each wire was periodically repeated along the growth direction. The atomic and electronic structures were converged with respect to the number of periodic repeat units along the growth direction, and it was found that, e.g., for [011] canted dihydride structures, four repeat units were sufficient to converge the energy per layer to within 0.2 eV (the band gap converges to 0.001 eV). For the initial structural relaxation, multiple repeat units were used rather than multiple k points to enable the surface to reconstruct into lower symmetry configurations. Once the structure was fully relaxed, the band structure, density of states, and effective masses were calculated using the smallest periodic repeat unit and a converged set of eight k points along the wire. The band structures were calculated using the ESPRESSO package.[37] For each NW, the supercell was chosen to be sufficiently large perpendicular to the growth direction to remove interactions between NWs. Supercells with sizes of 21.2, 31.8, and 42.3 Å were used for the 1.1, 2.0, and 3.0 nm diameter NWs, respectively. For all configurations, Hamann norm-conserving pseudopotentials[38] in the Kleinman-Bylander form[39] were used with a wave-function energy cutoff of 35 to 55 Ry (for both QBox and PWSCF calculations). The choice of energy cutoff was based on the convergence of eigenenergies (e.g., the band gap was converged to 0.001 eV), bond lengths (converged to less than 0.005 Å), and forces (the forces on each atom are less than 0.001 eV/Å).

In assessing the accuracy of using LDA-DFT, as well as the pseudopotentials, we performed calculations for the Si bulk and found that the predicted lattice constant and the Si-Si bond lengths are 5.43 and 2.35 Å, respectively, with 1% of experimental values. Furthermore, since the Si-Si bond lengths in the NW structures deviate only slightly from

TABLE I. The size, growth directions, and number of atoms for the canted surface structure NWs.

Size (nm)	Growth direction	No. of Si	No. of H
1.1	[001]	52	44
	[011]	64	48
	[111]	76	60
2.0	[001]	164	84
	[011]	232	112
	[111]	292	132
3.0	[001]	384	124
	[011]	520	144
	[111]	652	180

the bulk configuration, and all the Si atoms remain in a closed shell configuration with four nearest neighbors similar to the bulk structure, we anticipate that the LDA-DFT calculations will predict the stable nanowire structures to a similar level of accuracy to that of the bulk structure. Typically, after structural relaxations within LDA-DFT calculations, we observe a small ($<1\%$) change in S-Si bond lengths in the core of the NWs. The Si-H bonds relax by 1–5% depending on the structure.

We also note that for computation of such a large system as 3 nm, where the number of atoms can have up to 834 atoms, the codes are optimized for use on massively parallel supercomputers. Table I lists the number of atoms in each system.

After analyzing the total energies of the relaxed geometries of each NW, we found that the canted dihydride structure is more stable than the symmetric dihydride. For example, the [011] 1.1 nm symmetric dihydride structure is 0.037 eV/Si atom higher in energy than the [011] 1.1 nm canted dihydride structure, and we find it is not even metastable, i.e., the dihydride groups spontaneously cant at zero temperature. Similar enhanced stabilities of the canted surface structures were observed in all the NWs. Therefore, for the remainder of this paper we focus on a comparison of the more stable canted dihydride and reconstructed surface structures. In Sec. II, we show that the electronic properties of the NWs are sensitive to the choice of surface structure, and the reason for the difference in the gaps predicted here, compared to those predicted in Ref. 32, is the choice of a symmetric dihydride surface structure in that paper.

The stability of the canted dihydride structure arises from its larger H-H separation. In the symmetric dihydride, the distance between two H atoms, belonging to neighboring SiH_2 groups, is 1.41 Å. On the other hand, depending on the growth direction and NW diameter, the H-H separation in the canted dihydride structure ranges from 1.96 to 2.34 Å, resulting in smaller H-H repulsion, and a more stable structure. This observation agrees with the prediction by Northrup for bulk Si(100) surfaces,[40] where the canted dihydride is more stable than the symmetric dihydride. Because the surfaces of the NWs are faceted (as a result of the atomistic details of the structure), we also observe an additional stability of the canted dihydride structure due to the free rotation in opposite

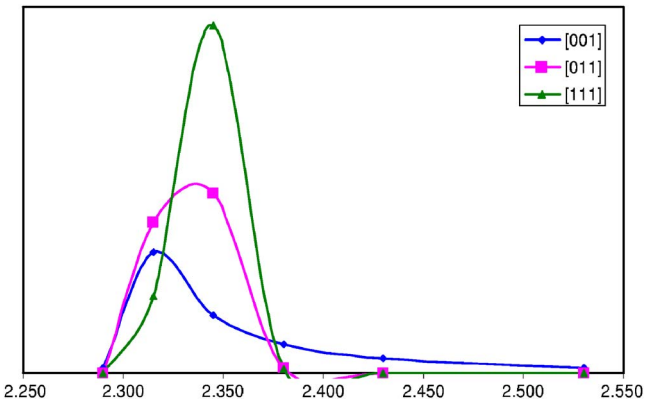

FIG. 2. (Color online) Bond length distributions for (2×1) surface-reconstructed 3 nm NWs with [001] (blue/diamond), [011] (pink/square), and [111] (green/triangle) growth directions in (Å).

directions of the SiH_2 group at the end of a surface facet, further reducing their H-H repulsion. This counter-rotation effect was first predicted to increase the stability of dihydride groups on the surfaces of hydrogen-terminated silicon quantum dots.[41]

We have also examined the deviation of the Si-Si bond lengths from the bulk silicon bond length for each of the NWs. We find a negligible deviation in bond length in the cores of the NWs (0.1%). On the surfaces there is a larger distribution of bond lengths with the largest deviations for the NWs with reconstructed surfaces. This difference is consistent with the intuition that surface reconstruction introduces strain into the system. It is also noticeable that NWs grown in the [001] direction with surface reconstructions have larger bond length distributions and lower symmetries than the other growth directions, [011] and [111]. The symmetry decreases from the [111] direction (point group of C_{3v}) to [011] (point group of C_{2h}) to [001] (one symmetry plane). Figure 2 illustrates the bond length distribution for (2×1) surface-reconstructed structures of 3 nm NWs with [001], [011], and [111] growth directions. While the Si-Si bond lengths for the [011] and [111] NWs range from 2.30 to 2.43 Å, those in the [001] NW have a larger range from 2.28 to 2.53 Å. For the canted dihydride structures, no significant differences in bond length distributions among the three growth directions were observed, supporting the conclusion that the canted dihydride surface structure introduces minimal strain into the silicon bonding network.

Currently, one of the major challenges to synthesizing nanomaterials is to control the structure and chemistry of the surface and then to characterize their surfaces. Typically, electron microscopy and x-ray diffraction can image the core of nanostructures and determine their crystal structure, but they lack the resolution to determine the structure of the surface. One of the most promising techniques for characterizing nanomaterial surface structures is x-ray absorption spectroscopy. In particular, extended x-ray absorption fine structure (EXAFS) measurements can distinguish between the core-level shifts of atoms in the core and on the surface of a nanomaterial. This allows the absorption spectrum of the surface atoms to be isolated and their structure analyzed. We have used the FEFF code,[42] which performs *ab initio*, self-

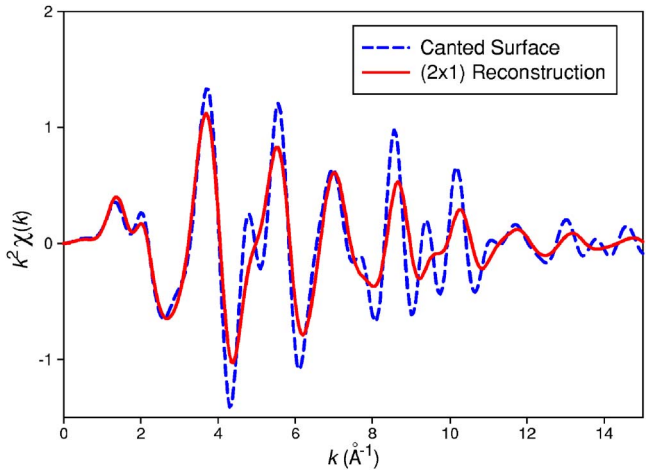

FIG. 3. (Color online) Predicted EXAFS absorption spectra for 2 nm NWs, grown along the [001] direction with canted and (2×1) reconstructed surfaces.

consistent, real space Green's function, atomic cluster calculations to predict the EXAFS absorption spectra of the NWs studied in this project. An example of the predicted EXAFS spectra for 2 nm diameter, [001] growth direction NWs with canted and reconstructed surfaces is shown in Fig. 3. The EXAFS spectra show a reduction in the amplitude of all the spectral peaks upon reconstruction. The absorption peaks at 5 and 9.5 Å^{-1} are also absent in the absorption spectra of the NW with the reconstructed surface. These changes in the EXAFS spectra due to surface reconstruction are observed for all the NWs studied here and could be used as evidence of a surface reconstruction taking place in NW samples.

In summary, we find that the canted dihydride surface structures has lower energy than the symmetric dihydride structures due to its reduced repulsion between nearest-neighbor surface SiH_2 groups. For NWs larger than 1 nm, it is also possible to reconstruct the 001-type surface facets. This reconstruction introduces strain into the system, which is most pronounced for NWs grown in the [001] direction.

II. STABILITIES OF THE RELAXED NANOWIRE STRUCTURES

To predict the relative stabilities of NWs with different diameters, growth directions, and surface structures, we calculated the free energy of formation, E_f, following the procedure described in Ref. 40,

$$E_f = E^{\text{tot}} + E_{\text{ZPE}} - n_{\text{Si}}\mu_{\text{Si}} - n_{\text{H}}\mu_{\text{H}}, \tag{2}$$

where E^{tot} is the total energy, E_{ZPE} is the zero-point energy of Si-H vibrations, n_{H} is the number of H atoms, and μ_{H} is the chemical potential of hydrogen. Since the temperatures considered here are much lower than the Si-H vibrational energy (~3000 K), only zero-point Si-H vibrations are included. Table II lists the critical temperatures, T_c, below which a canted dihydride surface structure is favored and above which a reconstructed surface with lower hydrogen content is favored. These temperatures are computed from the standard partition function, within the harmonic approximation, including both rotational and zero-point vibrational energies[43] at 1 atm of partial pressure. We find that the values of T_c are sensitive to the surface structure, size, and growth direction of the NWs. As an illustration, Fig. 4(a) shows the formation energies of 2 nm [001] NWs with three different surface structures (canted dihydride, partially reconstructed, and fully reconstructed) plotted as a function of the hydrogen chemical potential, μ_{H}. In the partially reconstructed structure, only the facets of the NWs are reconstructed, whereas in the fully reconstructed structure, both the facets and the edges are reconstructed.

It can be seen from Fig. 4(a) that the canted dihydride structure, with the highest coverage of hydrogen on the surface, and hence no reconstruction, has the lowest formation energy when $\mu_{\text{H}} > -0.23$ eV (or $T < 324$ K). These high μ_{H} conditions exist when the NWs are exposed to atomic H, which is generated from H_2 gas at appropriate

TABLE II. The sizes, growth directions, symmetry, critical temperature T_C at which the surface reconstructs, and the single-particle band gap of each of the NW studied.

Size (nm)	Growth direction	T_c (K)	Symmetry		Gap (eV)	
			canted	reconstructed	canted	reconstructed
1.1	[001]	350	C_2h	C_2h	2.35	2.03
	[011]	200	C_2h	C_2h	1.72	1.67
	[111]		C_3v		2.12	
1.2	[001]			C_s		1.95
	[011]	200	C_2h	C_2h		
	[111]	350	C_3v	C_3v		1.54
2.0	[001]	530	C_2h	C_s	1.32	0.78
	[011]	250	C_2h	C_2h	0.94	0.92
	[111]	250	C_3v	C_i	1.18	1.15
3.0	[001]	570	C_i	C_s	0.88	0.64
	[011]	200	C_2h	C_s	0.72	0.71
	[111]	320	C_3v	C_3v	0.85	0.84

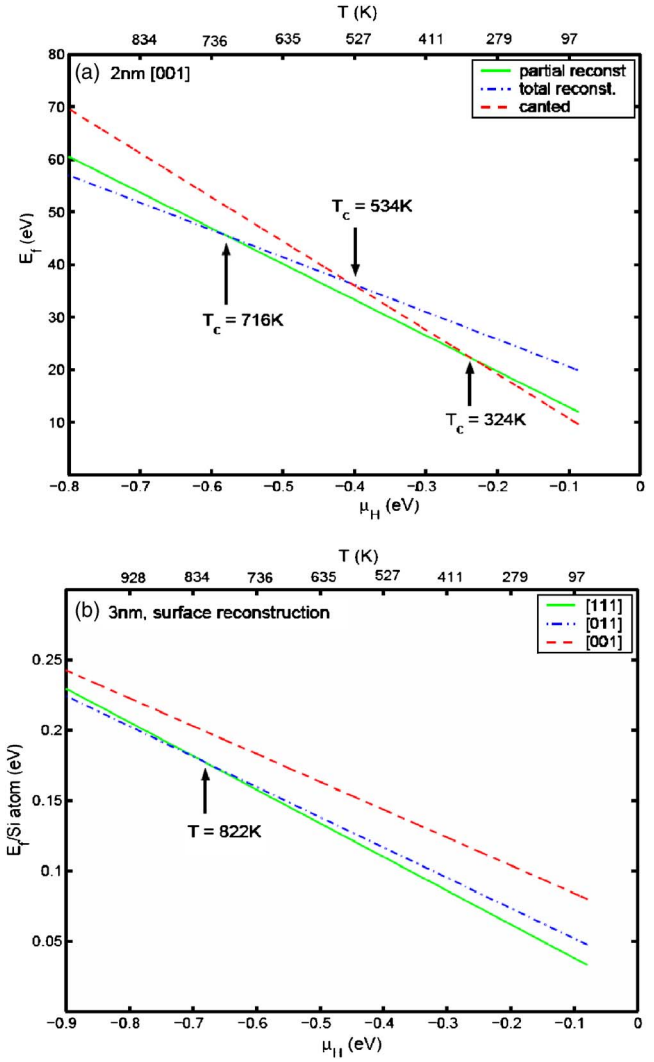

FIG. 4. (Color online) Relative stabilities of NWs: (a) 2 nm NWs with three different surface structures [canted dihydride (red dash line), partial reconstruction (green solid line), and total reconstruction (blue dash-dot line)] and (b) 3 nm (2×1)-reconstructed NWs in three different growth directions: [001] (red dash), [011] (blue dash-dot), and [111] (solid green).

conditions[44–46] or by HF etching.[47] For $\mu_H<-0.23$ eV, the partial (2×1) surface reconstruction becomes more favorable, and if $\mu_H<-0.58$ eV (or $T>716$ K), reconstructing surface steps to further reduce the hydrogen content produces the lowest formation energy.

Similarly, the dependence of the NW formation energy on growth direction is shown in Fig. 4(b), which shows E_f as a function of μ_H for NWs with the same diameter but different growth directions. The figure compares 3 nm NWs with a (2×1) surface reconstruction and [001], [011], and [111] growth directions. We note that the number of Si and H atoms per periodic repeat unit along the wire varies with the growth direction of the wire due to the atomistic details of the structures. Therefore, we plot the formation energy per Si atom (E_f/n_{Si}) as a function of chemical potential of hydrogen μ_H. This shows how the additional formation energy required to add a Si atom to the wire changes as a function of chemical potential of hydrogen surrounding. Figure 4(b) shows that the [111] growth direction is the most favorable direction for $T<822$ K (or $\mu_H>-0.7$ eV). Above 822 K, the [011] direction becomes more stable. For the [001] growth direction to be preferred, very high temperatures (or very low μ_H) would be required. It is worth noting that among the three growth directions, the wire structure with [001] growth direction and surface reconstruction has the lowest symmetry and the most strain, as mentioned above. This increased strain energy may explain why the [001] growth direction is energetically less favorable than the [011] and [111] directions. Similar trends showing [111] as the most favorable growth direction were also observed for the NWs with smaller diameters. For NWs with canted surface structures, the value of T_c at which the [011] becomes more favorable than [111] is $T>767$ K for 1.1 nm. For larger diameter (2 and 3 nm) NWs, [111] is found to be the preferred direction for most of the temperature range.

It is difficult to directly compare the most favorable growth directions predicted by thermodynamic formation energies [Eq. (2)] with those growth directions observed in experimental synthesis. NWs are synthesized either using the chemical vapor deposition (CVD) method with a metallic catalyst[1,4,5,46] or by vaporization of a mixture of Si and SiO_2.[3,9] Consequently, the observed growth direction, surface structure, and diameter of the NWs will depend on many factors such as the type and size of the catalyst, the substrate on which the NW is grown, the choice of chemical precursors, and any post-growth temperature treatments. Many of these parameters will affect the kinetics of the growth process, which are not included in a simple formation energy analysis. However, it is interesting to note that the favored growth directions most commonly reported in the literature are [111][1,2,5,46] and [110][46] and sometimes [112],[3,4,9,46] with the [111] growth direction most frequently observed, as predicted by our formation energy analysis.

III. ELECTRONIC PROPERTIES OF SILICON NANOWIRES

A. Electronic band structures

The effects of the size, surface structure, and growth direction on the electronic properties of NWs can be understood by analyzing the band structure, band gap, and density of states. As an illustration of the effect of growth direction, in Fig. 5 the electronic band structures of 1.1 nm NWs with canted dihydride surface structures and [001], [011], and [111] growth directions are compared. The band structures are shown along the growth direction of the wires. The band structures corresponding to the three growth directions in Fig. 5 reveal that, for these 1.1 nm NWs, all the band gaps are direct (at the Γ point). The conduction band (CB) for the case of [011] exhibits the largest dispersion, while the [001] and [111] directions exhibit only a small dispersion. From the Γ to X points, the separation between the CB and the valence bands (VB) increases significantly for the cases of [001] and [011] and is less pronounced for the case of [111]. The same characteristics hold for larger diameter NWs.

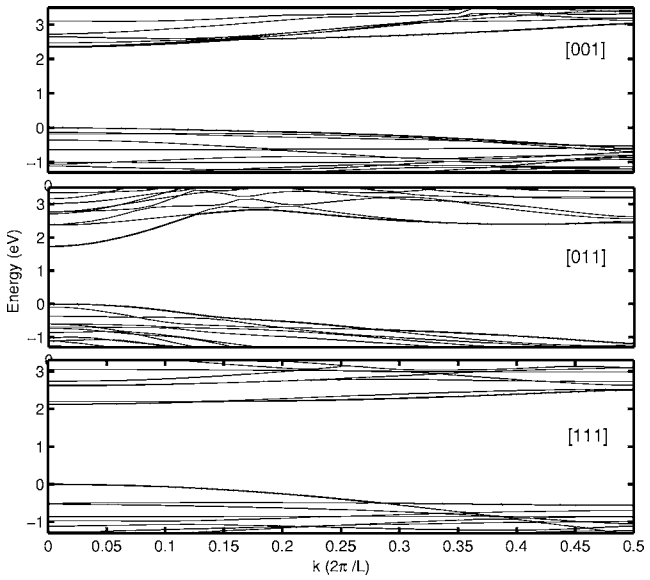

FIG. 5. Band structures of 1.1 nm canted dihydride NWs with three growth directions: (a) [001], (b) [011], and (c) [111]. The Fermi level is set to the top of the valence band.

To quantify the effects of quantum confinement on the electronic properties of the NWs, the band structures of NWs with the same surface structure and growth direction but different diameters are compared in Fig. 6. The figure shows the band structures of bulk silicon plotted along the [011] direction as well as the band structures of 1.1, 2.0, and 3.0 nm [011] NWs with canted dihydride surface structures. Bulk silicon has an indirect band gap, with the valence-band maximum (VBM) located at the Γ point and the conduction-band minimum (CBM) located approximately 85% from Γ to *X*. As the dimensions of silicon are reduced from the bulk to a NW geometry, quantum confinement will increase the energy of the CBM and decrease the energy of the VBM, thereby

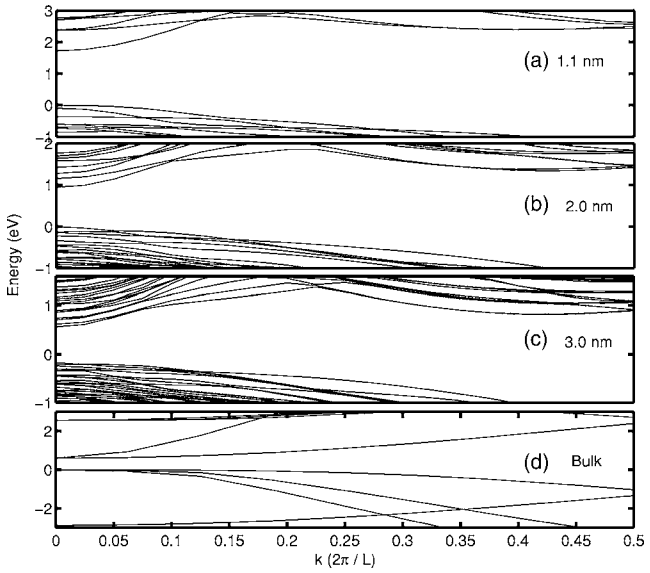

FIG. 6. Band structures of [011] canted dihydride NWs of various diameters [1.1 nm (a), 2 nm (b), and 3 nm (c)], and of bulk Si. Fermi level is set to the valence-band maximum.

increasing the band gap of the material. However, the magnitude of the energy shift produced by quantum confinement is different for each point in the band structure and depends on the effective mass and growth direction of the wire. The effective mass of electrons in bulk silicon is higher at the Γ point than at the *X* or *L* points. Therefore, from simple effective-mass theory one expects the CBM energy to increase more at the *X* and *L* points than at Γ. For nanostructures with sufficiently small dimensions, this difference in energy shifts at different points in the Brillouin zone is sufficiently large to move the CBM at the *X* and *L* points above the CBM at the Γ point. The nanostructure is then considered to have undergone a transition from an indirect to direct gap material. Our results show that in silicon NWs the critical size at which this indirect to direct transition takes place depends on the growth direction and surface structure of the NW.

We also note that a direct gap as discussed does not guarantee allowable transitions near the gap. We find that the magnitude of the oscillation strengths and the onset of the absorption peaks vary, depending on the size, surface structure, and growth direction. The detailed studies of this dependence are the subject of our next paper.

To directly compare the band structures of the NWs and bulk silicon, the band structure of bulk silicon in Fig. 6 is folded to be consistent with the size of the simulation supercell along the growth direction. Figure 6 shows that the band gaps of the NWs remain direct even for NWs with diameters up to 3 nm. The band gap is found to increase with decreasing diameter, consistent with the quantum confinement model. Similar band shifts have been observed in Refs. 27, 29, and 32. For [001] and [011] NWs, we found that the gap is still direct for NWs with diameters up to 3 nm. For [111] NWs, at a diameter of 2 nm the gap becomes indirect for NWs with canted dihydride surfaces but remains direct for NWs with a reconstructed surface. For the larger 3 nm wire, both the NWs with canted and reconstructed structures have indirect gaps.

B. Electronic band gaps

As Figs. 5 and 6 show, variations in NW diameter, surface structure, and wire growth direction all affect the size of the band gap of NWs. Figure 7 compares the dependence of NW band gaps on size and surface structure. As a reference, the band gap of bulk Si calculated within the LDA (0.54 eV) is also shown. For all growth directions, as the NW diameter decreases, the band gap increases as a result of quantum confinement. This general trend is observed for both canted dihydride and reconstructed surface structures. For the canted dihydride structures, when the diameter increases from 1.1 to 3 nm, the gap decreases from 2.35 to 0.88 eV for [001] NWs, from 1.72 to 0.72 eV for [011] NWs, and from 2.12 to 0.85 eV for [111] NWs. These observed trends in the size dependence of the band gap agree with those found by Zhao *et al.*[32] and Saita *et al.*[28] Zhao *et al.* predicted that the LDA band gap will decrease from 1.5 to 0.7 eV as the diameter increases from 1.2 to 4.0 nm for [011] NWs, and from 2.3 to 0.8 eV as the diameter increases from

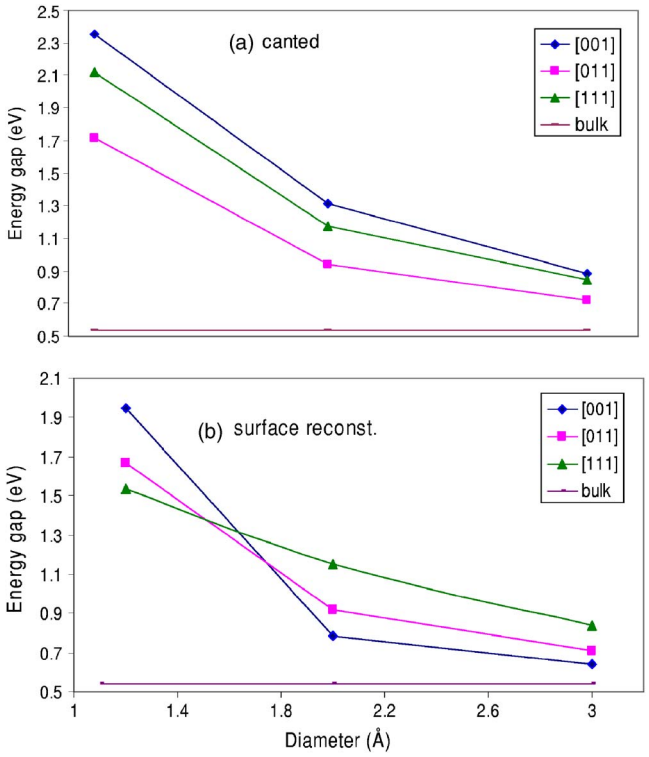

FIG. 7. (Color online) Energy band gap of NW with different growth directions as a function of NW diameter: (a) canted dihydride and (b) surface reconstructed.

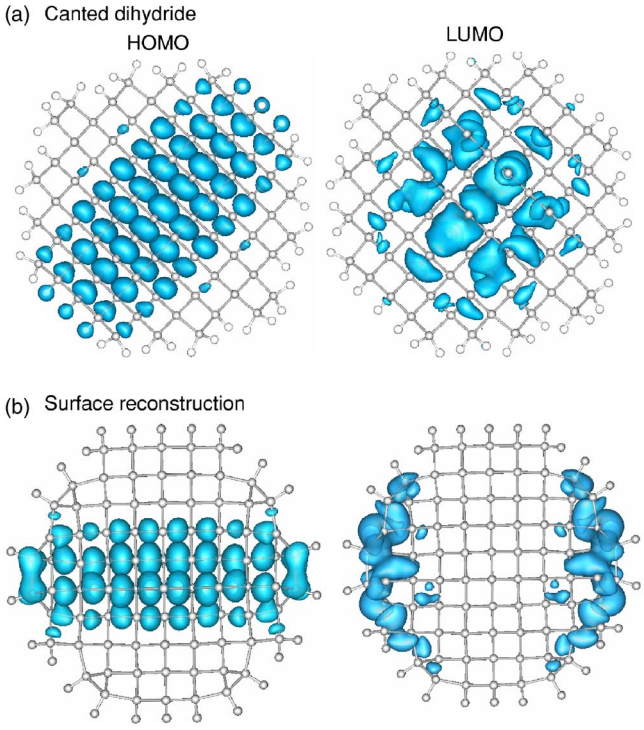

FIG. 8. (Color online) HOMO and LUMO orbital densities of 2 nm [001] NWs with different surface structures: (a) canted dihydride and (b) (2×1) surface reconstruction. The blue charge-density isosurfaces represent 64% of density.

0.9 to 3.2 nm for [111] NWs. For the 1.2 and 1.6 nm diameter [011] NWs, Zhao *et al.* also included the effects of GW corrections to the LDA band gap. These corrections increase the gaps of these two wires from 1.5 and 1.0 eV to 3.1 and 2.3 eV, respectively. Saita *et al.* found that for [111] NWs, the band gap varies from 2.83 to 1.90 eV as the diameter increased from 0.55 to 1.0 nm. The small differences between our LDA calculated gaps and those in Refs. 28 and 32 are attributed to our use of a higher cutoff energy and a canted, rather than symmetric, dihydride surface structure.

For the surface reconstructed structures, the gap varies from 2.03 to 0.64 eV for [001], from 1.67 to 0.71 eV for [011], and from 1.54 to 0.84 eV for [111]. Therefore, while the size dependence of the band gap for the canted dihydride structures is largest for the [001] growth direction, then [111], and finally [011], that order changes to [001], [011], and [111] for the reconstructed surface structures. In addition, for the same wire diameter and growth direction, the values of the band gap vary as the surface structure of the NWs changes. It is also noted that the difference in band gap for the canted structure and the reconstructed one is found to be largest for the case of [001]. For the [001] growth direction, surface modification leads to the formation of surface states, which result from the strain introduced by surface reconstruction. As the NW diameter approaches the bulk limit, the difference in the band gap due to the differences in growth directions or in surface structures decreases.

The effects of NW diameter, surface structure, and growth direction on the band-edge electronic properties of NWs can be understood in more detail by studying the highest occupied molecular orbital (HOMO) and lowest unnoccupied molecular orbital (LUMO). Figure 8 shows density plots of the HOMO and LUMO orbitals of 2 nm [001] NWs with canted dihydride and reconstructed surfaces. While the HOMOs of these two structures are similar in size and localization, the LUMOs are quite different. The LUMO of the canted dihydride structure is localized mostly in the core of the NW while the LUMO of the surface reconstructed structure is localized on the surface of the NW. This phenomenon has also been observed in hydrogen passivated silicon quantum dots with reconstructed surfaces.[41]

As discussed above, surface reconstruction introduces strain into the NWs, and among the three growth directions the [001] wires incur the most strain (see Fig. 2). We found that the surface states in the [001] NWs are related to the strain in the wires. Figure 8 shows that the surface states are located on the most strained facets of the NW. Those Si-Si bonds associated with the highest strain in the [001] NWs, where the LUMO is localized, are longer than 2.4 Å. Bonds of this length are not observed in [011] and [111] NWs, and hence no surface states are observed in the LUMO's of the surface reconstructed structures for these growth directions.

C. Nature of the band-edge orbitals

In addition to surface structure, changes in growth direction are also responsible for modification of the HOMO and LUMO densities. In Fig. 9, the HOMOs and LUMOs of 2 nm canted dihydride NWs with different growth directions are compared. The HOMO of the [111] NW has C_{3v} symme-

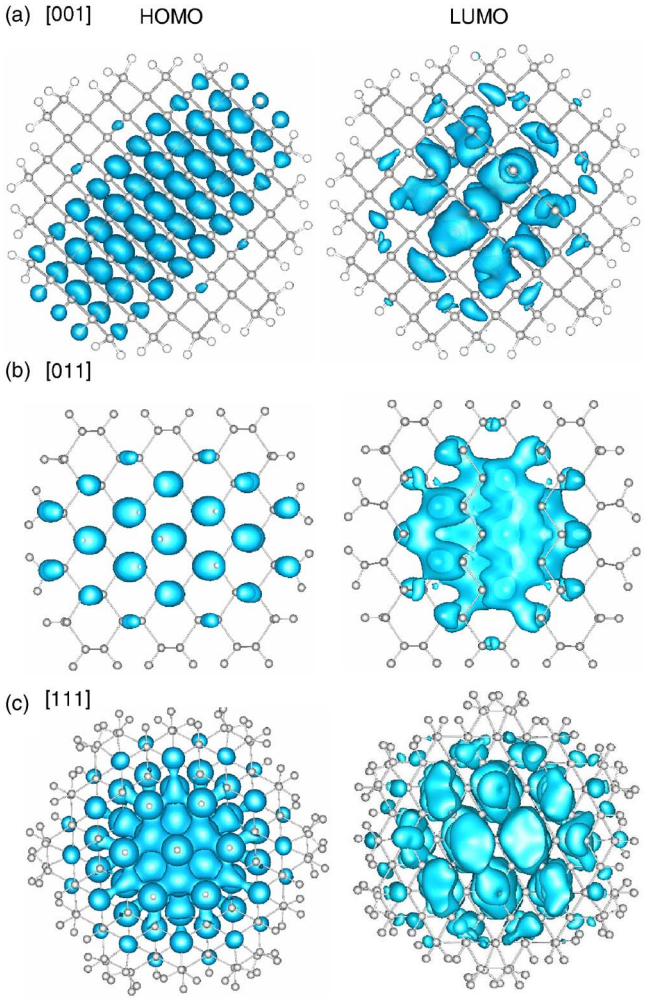

FIG. 9. (Color online) HOMO and LUMO of 2 nm canted dihydride NWs in three different growth directions: (a) [001], (b) [011], and (c) [111].

try while the HOMOs of the NWs with [001] and [011] growth directions exhibit C_{2h} symmetry. The different symmetries of the band-edge orbitals result from the relative orientation of the growth direction of the NW to the underlying crystal structure. Bulk silicon has T_d symmetry. As a wire is formed, this T_d symmetry is reduced by the formation of the surface and the presence of the passivated H atoms (see Table II). For example, for 3 nm NWs, the wire symmetry is C_i, C_{2h}, and C_{3v} for [001], [011], and [111], respectively.

Figure 10 shows the orientation of the Si-Si bonds with respect to the growth directions of the NWs. For [111] NWs, the hybridized sp^3 orbitals are oriented such that the C_3 axis is parallel to the growth axis of the NW, producing band-edge states with C_3 symmetry.

For [001] and [011] NWs, the Si-Si bonds are oriented such that the C_2 axis is parallel and perpendicular to the wire axis, respectively. For the [001] NW, when the surface structure is taken into consideration, the two Si atoms in the upper part of the tetrahedron (atoms labeled 1 and 2) (see Fig. 10) are not symmetry-equivalent to those in the lower part of the tetrahedron (atoms 3 and 4). Similarly, in the [011] NW the two atoms on the right-hand side of the tetrahedron (atoms 1 and 2) are not equivalent to those at the left of the tetrahedron (atoms 3 and 4). For the [001] case, the HOMO is formed from a linear combination of bonding states between atoms 3 and 4 and the central Si atom of the tetrahedron. This results in the distinctive orientation of the HOMO along this bonding direction. The HOMO-1 orbital is localized along the bonds between the central Si atom and atoms 1 and 2, i.e., perpendicular to the HOMO. Similarly, for the [011] NW the HOMO is localized on the bonds between atoms 1 and 2 and the central atom, and the HOMO-1 is localized on the bonds between atoms 3 and 4 and the central atom.

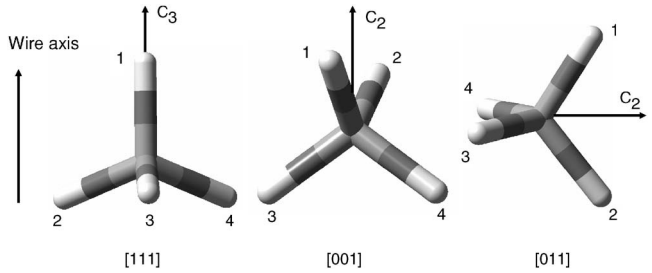

FIG. 10. Si-Si bond orientation in different growth directions.

While the influence of surface structures on the HOMO and LUMO density is remarkable, the effect of NW diameter

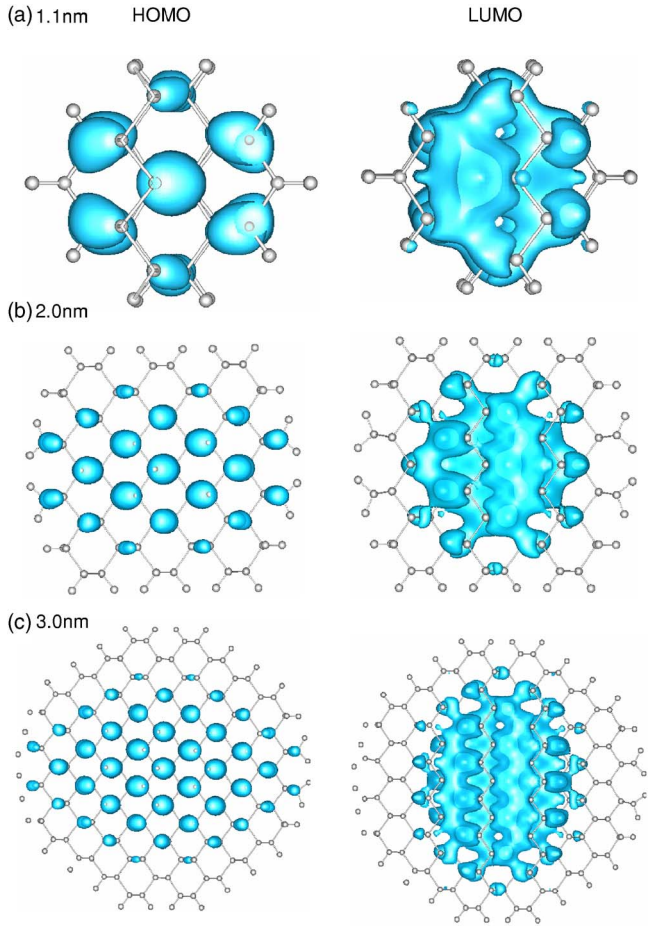

FIG. 11. (Color online) HOMO and LUMO of [011] surface reconstructed NWs with diameters 1.1, 2.0, and 3.0 nm.

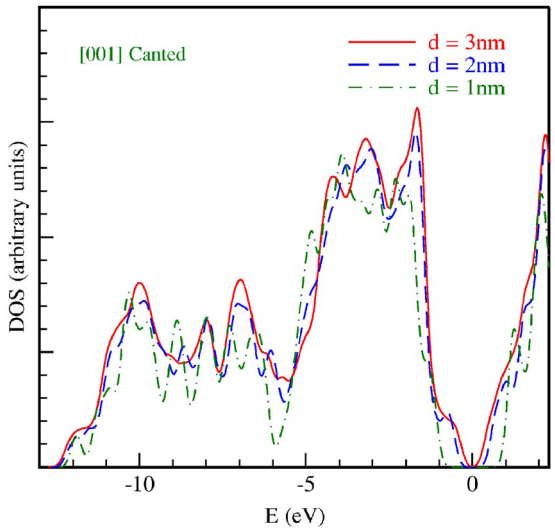

FIG. 12. (Color online) Density of states (DOS) of [001] canted dihydride NWs having diameters ranging from 1 nm (green dash-dot) to 3 nm (red solid).

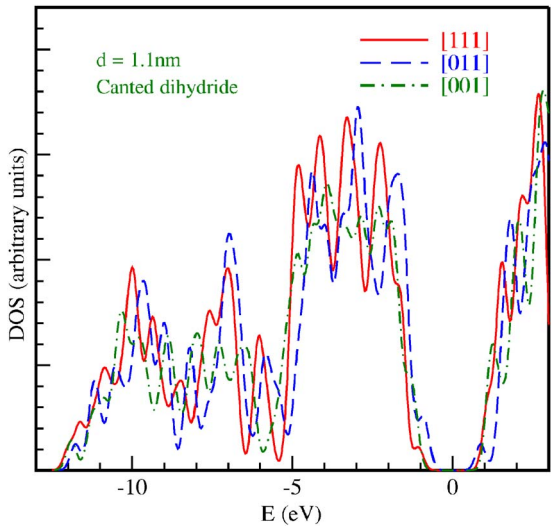

FIG. 13. (Color online) DOS of 1.1 nm canted dihydride NWs with three different growth directions ([111] red solid line, [011] blue dash line, and [001] green dash-dot).

on the shape of the HOMO and LUMO is much smaller. For example, Fig. 11 shows the HOMO and LUMO of [011] surface reconstructed NWs with diameters of 1.1, 2.0, and 3.0 nm. The shapes of the HOMO and LUMO evolve slowly with size, with similar shaped envelope functions as would be expected from simple effective-mass models. We note that as the hydrogen passivation of the surface provides a relatively small barrier for electrons and holes, the HOMO and LUMO orbitals spill out more from the core as the diameter is reduced.

Figure 12 shows the electronic density of states (DOS) of [001] canted dihydride NWs with diameters ranging from 1.1 to 3 nm. The energy gap as well as the separation between the CBM and VBM can be seen to decrease with increasing diameter. In the 1.1 nm NW, the discrete density of states present in a nanoscale material becomes more pronounced, producing a spiky DOS, and the bandwidth is reduced by 0.2 eV. These broad features hold for other growth directions. Similar variations in DOS are observed when the growth direction changes (see Fig. 13). At the band edges, the VBM is higher for the [011] NW than for [001] and [111].

In summary, we predict a decrease in band gap with increasing NW size for all NW growth directions, resulting from a reduction in quantum confinement. Surface reconstruction of the NW surfaces further reduces the band gap due to the creation of surface states, which arise from the strain introduced by the surface reconstruction. As the NW diameters decrease, the conduction-band minimum at the Γ point is blueshifted less than the *X* and *L* points. This results in a transition from indirect to direct band gaps. This direct to indirect transition occurs for [111] NWs larger than 2 nm and for [001] and [011] NWs larger than 3 nm. In addition to a size dependence of the band-edge states, differences in the underlying crystal structures result in differences in the symmetry of band-edge states.

D. Electron and hole effective masses

As expected, changes in the band structure and band gap with diameter, growth direction, and surface structure also

TABLE III. Calculated effective electron and hole masses (m_e^* and m_h^*) for different NW structures, growth directions, and diameters.

Size (nm)	Growth direction	m_e^*		m_h^*	
		canted	reconstructed	canted	reconstructed
1.1	[001]	0.72	0.34	1.19	0.75
2.0		0.40	0.34	0.83	0.50
3.0		0.33	0.38	0.70	0.48
1.1	[011]	0.14	0.13	0.44	0.27
2.0		0.12	0.12	0.17	0.18
3.0		0.14	0.13	0.23	0.23
1.2	[111]	4.78	0.53	0.20	0.18
2.0		2.74	2.00	0.15	0.14
3.0		0.47	0.54	0.12	0.12

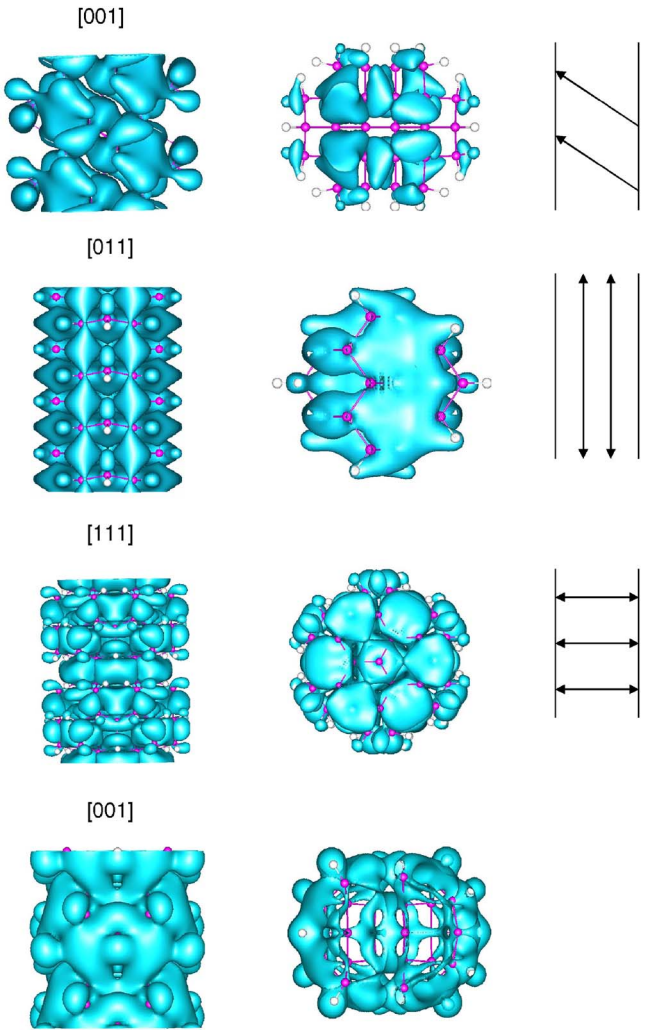

FIG. 14. (Color online) LUMO's of 1.1 nm canted dihydride NWs with three different growth directions. Charge-density isosurfaces (blue) represent 94% density. The arrows show the direction of wave propagation (and electron transport).

lead to changes in the effective mass of electrons and holes in the NWs. Table III lists the calculated effective electron and hole masses (m_e^* and m_h^*) for the different NW structures, growth directions, and diameters. It shows that the effective mass varies dramatically with the growth direction, NW size, and surface structure.

For NWs grown along the [001] direction, the effective mass decreases with increasing NW diameter, consistent with the trend found in Ref. 23. The trend can be explained qualitatively using effective-mass theory (EMT): In bulk silicon, there are six equivalent CB minima along the [100], [010], and [001] directions. As the wire is formed in the [001] direction, the CBMs in the $+z$ and $-z$ directions are shifted up by a large amount due to their small transverse mass. The other four CB minima are also shifted up but by a smaller amount because of their larger mass in the confinement direction. Therefore, the CBM of the [001] NW is derived from the states at the four minima along [100] and [010] perpendicular to the growth direction. In the limit of a large NW, the effective mass along the NW growth direction will be determined by the transverse bulk effective mass at these minima. In bulk silicon, this transverse effective electron mass is 0.19 eV within the LDA. Consequently, the electron effective masses of [001] NWs approach this bulk limit as their diameter increases; for canted surfaces the masses are 0.72, 0.67, 0.4, and 0.33 for 1.1, 1.2, 2.0, and 3.0 nm diameter wires, respectively. However, for [001] NWs with reconstructed surfaces, we observe only a small change of effective mass with NWs size: the values of m_e^* are 0.34, 0.34, and 0.38 for 1.1, 2.0, and 3.0 nm NWs. This weak size dependence results from a change in the HOMO and LUMO of the wire upon surface reconstruction.

Similarly, the effective electron masses of [011] NWs are almost independent of NW diameter and surface structure. The electron mass is found to be almost constant (0.12–0.14), and the hole mass varies from 0.17 to 0.44. We note that the effective electron and hole masses for NWs grown in the [011] direction are even smaller than those of bulk silicon. This may produce higher electron and hole mobilities for NWs grown in these directions and supports the motivation for using these NWs as components in a composite thermoelectric material. We also note that a recent work on Si NWs reveals that Si NWs can have conductivity as high as that of doped Si bulk,[48] and hence it would be interesting to study the dependence of the mobility of pure Si and doped Si NWs on their size, surface structures, and growth direction.

For NWs grown in the [111] direction, we also observe a size dependence of effective mass due to quantum confinement. However, for the case of surface reconstructed [111] NWs, a large value of m^* occurs for the case of 2 nm. The anomaly is attributed to symmetry breaking caused by reconstruction at this NW size. The symmetry of the 2 nm NW is only C_i, while that of the NWs of diameters 1.2 and 3 nm is C_{3v}.

To understand the dependence of the effective mass on growth direction, the HOMOs and LUMOs of 1.1 nm [001] and [011] NWs and a 1.2 nm [111] NW with canted dihydride surface are shown in Fig. 14. The LUMO of the [011] NW is most delocalized along the growth direction. This is consistent with the large dispersion in the band structure along the wire and the low electron effective mass. For [011] nanowires, the LUMO is formed by horizontal delocalized planes coupled through chains along the growth direction. In the [001] and [111] NWs, the LUMOs form delocalized chains diagonal and perpendicular to the growth direction (see the schematic figures on the right-hand side of Fig. 14).

The difference in the direction of delocalization of the LUMOs is related to the underlying crystal structure. For [011] NWs, in the LUMO the horizontal delocalization is observed on the central atom and symmetry-equivalent atoms 3 and 4. These planes are coupled by delocalization on the symmetry-equivalent atoms 1 and 2 (see Fig. 10) which are aligned with the growth direction, producing electron tunneling along the wire and a low effective mass along the growth direction. In [111] NWs, the LUMO is delocalized in the plane of atoms 2, 3, and 4. This plane is perpendicular to the growth direction resulting in a weak coupling along the wire and a heavy electron mass.

Similarly, the small value of the effective mass for the 1.1 nm [001] NW with a surface reconstructed case results

from the dramatic change in the LUMO due to the surface reconstruction. As a result of surface modification, the LUMO changes from being delocalized diagonally with respect to the growth axis to forming zigzag chains that are delocalized along the wire axis (see Fig. 14).

IV. CONCLUSIONS

In conclusion, we have used first principles electronic structure calculations to systematically investigate the relative stability and electronic properties of silicon NWs with different surface structures [symmetric and canted dihydrides and (2×1) reconstructions], growth directions, and diameters. NWs grown in the [111] direction are predicted to be the most thermodynamically stable over a wide range of temperatures. The electronic properties, including band gaps, band structures, and effective masses, are found to depend sensitively on all the NW structural parameters. The size dependence of the band gap depends on the growth direction of the NW, and the band gaps for a given size also depend on surface structure. NWs with reconstructed surfaces have LUMO orbitals localized on the reconstructed facets and exhibit smaller band gaps. Effective masses of NWs grown in the [001] direction decrease monotonically with size, approaching the bulk transverse effective mass for large wires. NWs with [011] growth directions exhibit a much weaker size dependence of the effective mass.

These calculations demonstrate the extremely rich nature of the electronic properties of silicon NWs. By changing the growth direction and NW diameter, or tuning the surface structure via chemical etching or heat treatment, it is possible to engineer NWs with a wide range of technologically important electronic properties. In principle, it is also possible to further increase the tunability of NW electronic properties by alloying the silicon NWs with other elements, such as germanium. We are currently investigating this possibility.

ACKNOWLEDGMENTS

We would like to thank Francois Gygi for providing us with QBox codes. We would also like to thank David Prendergast for providing the parallelized PWSCF codes and Tadashi Ogitsu for help in developing QBox utilities. This work was performed under the auspices of the U.S. Department of Energy by the University of California, Lawrence Livermore National Laboratory under Contract No. W-7405-Eng-48.

*Electronic address: williamson10@llnl.gov

[1] S. Sharama, T. Kamin, and R. Williams, Appl. Phys. A **80**, 1225 (2005).
[2] M. Saifislam, S. Sharama, T. Kamins, and R. Williams, Appl. Phys. A **80**, 1133 (2005).
[3] Y. Zhang, Y. Tang, N. Wang, C. Lee, I. Bello, and S. Lee, J. Cryst. Growth **197**, 136 (1999).
[4] X. Yan *et al.*, J. Cryst. Growth **257**, 69 (2003).
[5] A. Hochbaum, R. Fan, R. He, and P. Yang, Nano Lett. **5**, 457 (2005).
[6] L. Canham, Appl. Phys. Lett. **57**, 1046 (1990).
[7] D. Katz, T. Wizansky, and O. Milo, Phys. Rev. Lett. **89**, 086801 (2002).
[8] X. Duan, J. Wand, and C. Lieber, Appl. Phys. Lett. **76**, 1116 (2000).
[9] D. Ma, C. Lee, C. Au, S. Tong, and S. Lee, Science **299**, 1874 (2003).
[10] X. Duan, Y. Huang, Y. Cui, J. Wang, and C. Lieber, Nature (London) **409**, 66 (2001).
[11] Y. Cui, Z. Zhong, D. Wang, W. Wang, and C. Lieber, Nano Lett. **3**, 149 (2003).
[12] Y. Cui and C. Lieber, Science **291**, 851 (2001).
[13] J. Hahm and C. Lieber, Nano Lett. **4**, 51 (2004).
[14] Y. Cui, Q. Wei, H. Park, and C. Lieber, Science **293**, 1289 (2001).
[15] A. Abramson, W. Kim, S. Huxtable, H. Yan, Y. Wu, A. Majumdar, C. Tien, and P. Yang, J. Microelectromech. Syst. **13**, 505 (2004).
[16] M. Dresselhaus, G. Dresselhauss, X. Sun, Z. Zhang, S. Cronin, and T. Koga, Phys. Solid State **41**, 679 (1999).
[17] S. Kubakaddi and B. Mulimani, J. Appl. Phys. **58**, 3643 (1985).
[18] A. Majumdar, Science **303**, 777 (2004).
[19] A. Majumdar, J. Microelectromech. Syst. **13**, 505 (2004).
[20] L. Hicks, Appl. Phys. Lett. **63**, 3230 (1993).
[21] L. Hicks and M. Dresselhaus, Phys. Rev. B **47**, 16631 (1993).
[22] X. Sun, Z. Zhang, and M. Dresselhaus, Appl. Phys. Lett. **74**, 4005 (1999).
[23] O. Rabin, Y. Lin, and M. Dresselhaus, Appl. Phys. Lett. **79**, 81 (2001).
[24] A. Khitun, A. Balandin, and K. Wang, Superlattices Microstruct. **26**, 181 (1999).
[25] L. Hicks and M. Dresselhaus, Phys. Rev. B **47**, 12727 (1993).
[26] L. Hicks, T. Harman, X. Sun, and M. Dresselhaus, Phys. Rev. B **53**, R10493 (1996).
[27] Y. Zheng, C. Rivas, R. Lake, K. Alam, T. Boykin, and G. Klimeck, IEEE Trans. Electron Devices **52**, 1097 (2005).
[28] A. Saita, F. Buda, G. Fiumara, and P. Giaquinta, Phys. Rev. B **53**, 1446 (1996).
[29] F. Buda, J. Kohanoff, and M. Parinello, Phys. Rev. Lett. **69**, 1272 (1992).
[30] J. Xia and K. Cheah, Phys. Rev. B **55**, 15688 (1997).
[31] T. Ohno, K. Shiraishi, and T. Ogawa, Phys. Rev. Lett. **69**, 2400 (1992).
[32] X. Zhao, C. Wei, L. Yang, and M. Chou, Phys. Rev. Lett. **92**, 236805 (2004).
[33] A. Read, R. Needs, K. Nash, L. Canham, P. Calcott, and A. Qteish, Phys. Rev. Lett. **69**, 1232 (1992).
[34] C.-Y. Yeh, S. Zhang, and A. Zunger, Phys. Rev. B **50**, 14405 (1994).
[35] S. Ossicini, C. M. Bertoni, M. Biagini, A. Lugli, G. Roma, and O. Bisi, Thin Solid Films **297**, 154 (1997).
[36] F. Gygi, *The QBox Code*, LLNL (2004).

[37] S. Baroni *et al.*, *The PWSCF Code* (2005), http://www.pwscf.org/
[38] D. Hamann, Phys. Rev. B **40**, 2980 (1989).
[39] L. Kleinman and D. Bylander, Phys. Rev. Lett. **4**, 1425 (1982).
[40] J. Nothup, Phys. Rev. B **44**, 1419 (1991).
[41] A. Puzder, A. Williamson, A. Reboredo, and G. Galli, Appl. Phys. Lett. **91**, 157405 (2003).
[42] A. L. Ankudinov, B. Ravel, J. Rehr, and S. Conradson, Phys. Rev. B **58**, 7565 (1998).
[43] G. Rushbrooke, *Introduction to Statistical Mechanics* (Clarendon Press, Oxford, 1957).
[44] A. Laracuente and L. Whitman, Surf. Sci. **545**, 70 (2003).
[45] A. Laracuente and L. Whitman, Surf. Sci. **476**, 247 (2001).
[46] Y. Wu, Y. Cui, L. Huynh, J. Barrelet, D. Bell, and C. Lieber, Nano Lett. **4**, 433 (2003).
[47] G. Belomoin, J. Therrien, and M. Nayfeh, Appl. Phys. Lett. **77**, 779 (2000).
[48] J.-Y. Yu, S.-W. Chung, and J. Heath, J. Phys. Chem. B **104**, 11864 (2000).